annalen der physik
www.ann-phys.org

Realization of Z_2 Topological Metal in Single-Crystalline Nickel Deficient NiV_2Se_4

Sitaram Ramakrishnan, Shidaling Matteppanavar, Andreas Schönleber, Bikash Patra, Birender Singh, Arumugam Thamizhavel, Bahadur Singh,* Srinivasan Ramakrishnan,* and Sander van Smaalen**

Temperature-dependent electronic and magnetic properties are reported for nickel-deficient NiV_2Se_4. Single-crystal X-ray diffraction shows it to crystallize in the monoclinic Cr_3S_4 structure type with space group $I2/m$ and vacancies on the Ni site, resulting in the composition $Ni_{0.85}V_2Se_4$ in agreement with our electron-probe microanalysis. Structural distortions are not observed down to 1.5 K. Nevertheless, the electrical resistivity shows metallic behavior with a broad anomaly around 150–200 K that is also observed in the heat capacity data. This anomaly indicates a change of state of the material below 150 K. It is believed that this anomaly could be due to spin fluctuations or charge-density-wave fluctuations, where the lack of long-range order is caused by vacancies at the Ni site of $Ni_{0.85}V_2Se_4$. The non-linear temperature dependence of the resistivity as well as an enhanced value of the Sommerfeld coefficient $\gamma = 104.0\,(1)$ mJ mol^{-1} K^{-2} suggest strong electron–electron correlations in this material. First-principles calculations performed for NiV_2Se_4, which are also applicable to $Ni_{0.85}V_2Se_4$, classify this material as a topological metal with $Z_2 = (1;110)$ and coexisting electron and hole pockets at the Fermi level. The phonon spectrum lacks any soft phonon mode, consistent with the absence of periodic lattice distortion in the present experiments.

1. Introduction

Topological metals such as Dirac and Weyl semimetals represent exotic quantum materials with non-trivial band crossings at the charge neutrality point in the bulk band structure that lead to peculiar quasi-particle excitations and physical properties. There has been a surge of interest in realizing these topological metals, owing to their novelty for fundamental science and device applications.[1,2] Here, we show that nickel-deficient $Ni_{0.85}V_2Se_4$ is a topological metal with $Z_2 = (1;110)$ based on first-principles calculations. Our bulk measurements on single-crystalline $Ni_{0.85}V_2Se_4$ show unusual quasi-particle excitations. The presence of vacancies is a common feature of compounds AT_2X_4 (A and T are transition metals; X is chalcogenide), which display exotic electronic and magnetic properties.

Cubic thiospinels of the type AT_2S_4 (A = Cu, Ni; T = V, Rh, Ir) have attracted attention due to the unusual ground states exhibited by them.[3–8] For instance, superconductivity (e.g., in $CuRh_2S_4$),[3] magnetic order in insulators ($CuIr_2S_4$)[4,5] and charge density waves (CDWs; CuV_2S_4)[6,7] have been found to exist in this class of compounds. It is worthwhile to recall here that the CDW in CuV_2S_4 was suppressed in as-grown crystals, because of the presence of defects.[9] In addition, structural studies have shown that phase transitions are accompanied by charge

S. Ramakrishnan
Department of Quantum Matter
AdSE
Hiroshima University
Higashi-Hiroshima 739-8530, Japan
E-mail: ramakris@hiroshima-u.ac.jp

S. Matteppanavar, B. Patra, B. Singh, A. Thamizhavel, B. Singh, S. Ramakrishnan
Department of Condensed Matter Physics and Materials Science
Tata Institute of Fundamental Research
Mumbai 400005, India
E-mail: bahadur.singh@tifr.res.in; ramakrishnan@iiserpune.ac.in

A. Schönleber, S. van Smaalen
Laboratory of Crystallography
University of Bayreuth
95447 Bayreuth, Germany
E-mail: smash@uni-bayreuth.de

The ORCID identification number(s) for the author(s) of this article can be found under https://doi.org/10.1002/andp.202200611

DOI: 10.1002/andp.202200611

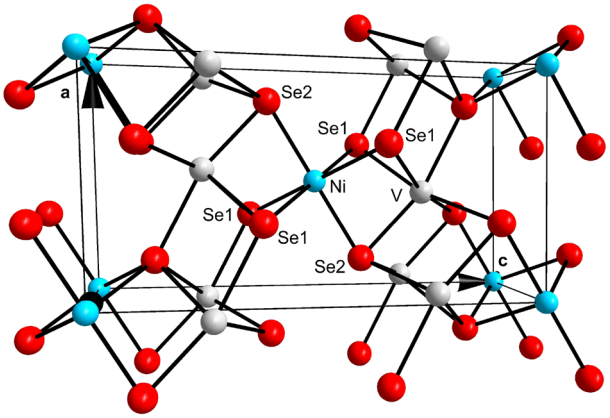

Figure 1. Crystal structure of $Ni_{0.85}V_2Se_4$ in a perspective view along **b**. The shortest distances between metal atoms form an unbounded network on the (1 0 1) plane; d(Ni–V) = 2.988 (1) Å and d(V–V) = 3.033 (1) Å at room temperature. The next shortest metal distance is b = 3.4327 Å along [0, 1, 0].

ordering and spin dimerization.[8] The occurrence of spin dimerization in a 3D compound, like $CuIr_2S_4$, is unique and not understood at present.

Apart from these cubic spinel compounds, there exists more than 50 chalcogenides with the same stoichiometry AT_2X_4 (A = Y, Cr, Fe, Co, Ni; T = Ti, Y, Cr; X = S, Se, Te), but crystallizing in the monoclinic defect NiAs structure type (**Figure 1**),[10] where very little investigations have been made. When we consider the band structures of compounds with the defect NiAs structure, we find that only octahedral site ions (both Ni and other transition metal) are involved. Unlike spinels, all metal ions are on octahedral sites and, therefore, the t_{2g} levels have the lowest energy. The metallic behavior for the AT_2X_4 compounds can be ascribed to partially filled bands formed as a result of T–T overlap. The NiAs structure is also known as the Cr_3S_4 structure type (space group $I2/m$) with two nonequivalent crystallographic sites for Cr. Chromium atoms occupy Wyckoff positions 2a and 4i, with two and four atoms per unit cell, respectively. These sites can be occupied by different elements.[11–19]

A study on polycrystalline NiV_2S_4 has indicated a CDW transition at 165 K,[20] while another study on NiV_2Se_4 reported a small anomaly in the resistivity around 160 K.[21] Using the vapor transport method, we have obtained a Ni-deficient single crystal of composition $Ni_{0.85}V_2Se_4$, which has the same crystal structure as NiV_2Se_4. Band structure calculations reveal that it is a Z_2 topological metal. Our experimental studies on the physical properties of $Ni_{0.85}V_2Se_4$ single crystal unfold an unusual electronic ground state of this material with exotic properties.

2. Results and Discussion

2.1. Evidence of Vacancies and Absence of Lattice Distortion

Single-crystal X-ray diffraction (SXRD) data were processed by Eval15[22] and SADABS.[23] All diffraction maxima could be indexed by a single unit cell with lattice parameters a = 6.1453(3) Å, b = 3.4327(2) Å, c = 11.5901(4) Å, and β = 91.619(3) deg, similar to the published unit cell of NiV_2Se_4.[24] Crystal structure refinements were done with Jana2006[25] with the monoclinic space group $I2/m$. **Table 1** shows the structural analysis for three different models on basis of the occupancy of the Ni site, in order to determine whether there are vacancies on the Ni site or there exists Ni/V disorder.

Table 1. Summary of results of refinements against SXRD data at 298 K for three structure models, differing in the treatment of the occupancy of the Ni site.

Model	I	II	III
Composition	NiV_2Se_4	$Ni_{0.4178(143)}V_{2.5822}Se_4$	$Ni_{0.8524(35)}V_2Se_4$
Occ[Ni]	1	0.4178(143)	0.8524(35)
Occ[V]	1	1	1
Occ[V_{Ni}]	-	0.5822	-
Unique reflections (obs/all)	578/685	578/685	578/685
No. of parameters	24	25	25
R_F(obs)	0.0317	0.0213	0.0209
wR_F(all)	0.0454	0.0253	0.0255
GoF (obs/all)	2.65/2.45	1.46/1.37	1.43/1.34
$\Delta\rho_{min}$, $\Delta\rho_{max}$(e Å^{-3})	−2.87, 1.49	−1.07, 1.30	−1.08, 1.28

Initially, model I was tested where the Ni site is completely filled. The composition is NiV_2Se_4 and it leads to a good fit of the diffraction data with R = 0.0317. In model II, a Vanadium atom (V_{Ni}) was introduced on the Ni site, such that the sum of the occupancies remains 1, Occ[Ni] + Occ[V_{Ni}] = 1. Refinement of Occ[V_{Ni}] then leads to a significant improvement of the fit, with R = 0.0213. However, the chemical composition derived from model II (Table 1) is not in agreement with the composition $Ni_{0.925(9)}V_{2.054(7)}Se_4$ found by an electron probe micro-analyzer (EPMA). Such a large difference in the measured compositions between SXRD and EPMA led us to believe that the partially filled site of Ni is not occupied by V. Therefore, model II is not suitable. Model III involves vacancies at the Ni site. Refinement of the occupancy of Ni results in an even better fit to the data, with R = 0.0209. Moreover the chemical composition of model III is in agreement with that obtained by EPMA, with a difference of about 7% deemed acceptable. One can also notice the standard uncertainty (su.) in the refined occupancy of Ni in model III is four times smaller than in model II. Our findings from SXRD and EPMA suggest that there is a 15% vacancy on the Ni site. **Table 2** provides the atomic coordinates and atomic displacement parameters (ADPs) of model III.

From the measured diffraction data at 298 K and at 100 K, reciprocal layers were reconstructed for 0kl, hk0, and h0l (Figures S1–S3, Supporting Information[26]). They demonstrate that, upon cooling the crystal down to 100 K, there are no superlattice reflections observed and there is no change to the lattice, indicating the absence of a CDW phase transition. **Table 3** shows the crystallographic information of the crystal at 298 and 100 K, respectively, as based on model III. For details regarding data processing of the 100 K data refer Section S1, Supporting Information.[26] The absence of the CDW transition is substantiated by our band structure calculations described in Section 2.2.

Table 2. Structural parameters for the monoclinic structure of crystal A of $Ni_{0.85}V_2Se_4$ at 298 K. Given are the fractional coordinates x, y, z of the atoms, their anisotropic displacement parameters (ADPs) U_{ij} ($i,j = 1, 2, 3$) and the equivalent isotropic displacement parameter U^{eq}_{iso}. All atomic sites, except Ni, are fully occupied.

Atom	Occ	x	y	z	U_{11}	U_{22}	U_{33}	U_{12}	U_{13}	U_{23}	U^{eq}_{iso}
Ni	0.8524(35)	0	0	0	0.0158(3)	0.0019(4)	0.0017(4)	0	0.0011(3)	0	0.0175(2)
V	1	−0.0451(1)	0	0.2556(1)	0.0133(2)	0.0021(3)	0.0153(3)	0	−0.0006(2)	0	0.0166(2)
Se1	1	0.3373(1)	0	0.3641(1)	0.0119(2)	0.0146(1)	0.0176(2)	0	−0.0003(1)	0	0.0015(1)
Se2	1	0.3381(1)	0	0.8924(1)	0.0138(1)	0.0153(2)	0.0163(2)	0	−0.0004(1)	0	0.0152(1)

Table 3. Crystallographic data of crystal A of $Ni_{0.85}V_2Se_4$ at 298 K and 100 K. Notice that space group $I2/m$ is a non-standard setting of space group No. 12 with standard setting $C2/m$.[27]

Temperature [K]	298	100
Crystal system	Monoclinic	Monoclinic
Space group	$I2/m$	$I2/m$
Space group no.	12	12
a (Å)	6.1453(3)	6.1314(2)
b (Å)	3.4327(2)	3.4174(3)
c (Å)	11.5901(4)	11.5462(3)
β (deg)	91.619(3)	91.741(3)
Volume [Å^3]	244.45(3)	241.83(3)
Z	2	2
Wavelength [Å]	Ag-Kα	Ag-Kα
Detector distance [mm]	100	100
2θ-offset [deg]	0	0, 30
Rotation per image [deg]	1	1
$(\sin(\theta)/\lambda)_{max}$ [Å^{-1}]	0.683589	1.009913
Absorption, μ [mm^{-1}]	19.271	19.469
T_{min}, T_{max}	0.5796, 0.8622	0.6018 0.8627
Criterion of observability	$I > 3\sigma(I)$	$I > 3\sigma(I)$
Number of reflections		
measured	4410	8970
unique (obs/all)	451/470	841/1024
R_{int} (obs/all)	0.0312/0.0321	0.0407/0.0415
Composition	$Ni_{0.8524(35)}V_2Se_4$	$Ni_{0.8488(25)}V_2Se_4$
No. of parameters	25	25
Occ[Ni]	0.8524(35)	0.8488(25)
R_F (obs)	0.0209	0.0196
wR_F (all)	0.0255	0.0246
GoF (obs/all)	1.43/1.34	1.32/1.21
$\Delta\rho_{min}$, $\Delta\rho_{max}$ [e Å^{-3}]	−1.08, 1.28	−1.27, 1.71

2.2. Structural Stability and Electronic Structure

We now discuss the stability and nontrivial state of NiV_2Se_4 with regards to the calculated band structure (**Figure 2**). These results also apply to $Ni_{0.85}V_2Se_4$, because the major effect of the introduction of vacancies is a shift of the Fermi level, which is presented in Section S3, Supporting Information. The results on Ni-deficient material show a 50 meV downward shift of the Fermi level as compared to pristine NiV_2Se_4. The phonon dispersion curves and associated phonon density of states (PDOS) are shown in Figure 2a. The absence of imaginary phonon frequency in the full BZ ensures that NiV_2Se_4 is dynamically stable. Moreover, the absence of a soft phonon mode indicates the absence of a structural instability or a periodic lattice distortion, as it would be expected in CDW materials, in agreement with the experiments. The PDOS suggests that Ni and Se atoms contribute to low-lying phonon modes, whereas the V and Se atoms dominate the high-frequency phonon modes.

The bulk band structure along the high-symmetry directions in the BZ of NiV_2Se_4 is shown in Figure 2b without spin-orbit coupling (SOC). It is metallic, where both the valence and conduction bands cross the Fermi level. Notably, the valence and conduction bands cross along Γ–C, M–D, D–A directions at generic **k** points close to the Fermi level, as indicated by red circles. The crossing points are stable against band hybridization to realize nodal line crossings. The band structure in presence of SOC is shown in Figure 2c. Although the system remains metallic, the band crossing points are now gapped, separating the valence and conduction bands locally at each **k** point. The orbital resolved band structure in Figure 2d shows that these band crossing points are composed of Ni–d, V–d, and Se–p orbitals. The existence of local band gap allows the computation of the Z_2 invariants (ν_0 ; $\nu_1\nu_2\nu_3$) in a manner similar to Z_2 topological insulators. Since NiV_2Se_4 crystal respects inversion symmetry, we can calculate the Z_2 invariants (ν_0 ; $\nu_1\nu_2\nu_3$) from the parity eigenvalues of the valence bands at each time-reversal-invariant momentum (TRIM) point.[28] The product of the parity eigenvalues of the occupied bands at the eight TRIM points is shown in Figure 2e. The calculated Z_2 of (1;110) indicates that NiV_2Se_4 is Z_2 topological metal. The topological phases are immune to the effects of a Hubbard U for the Ni and V atoms, as discussed in Section S4, Supporting Information.

The nontrivial state is further demonstrated by calculations of the surface electronic structure. They reveal a single Dirac cone topological state present within the energy gap of the bulk band structure (see Section S3, Supporting Information, for details[26]). Figure 2f–h shows the calculated Fermi surface of NiV_2Se_4. Owing to the multiband crossings at the Fermi level, the Fermi surface consists of both electron and hole bands which are shown separately in Figure 2f,g, respectively. The metallic behavior is consistent with the experimental measurements.

2.3. Electrical Resistivity

The electrical resistivity, $\rho(T)$, of $Ni_{0.85}V_2Se_4$ decreases upon cooling from room temperature down to 1.5 K (**Figure 3**). In particular, a broad hump is observed between 150 and 200 K, which

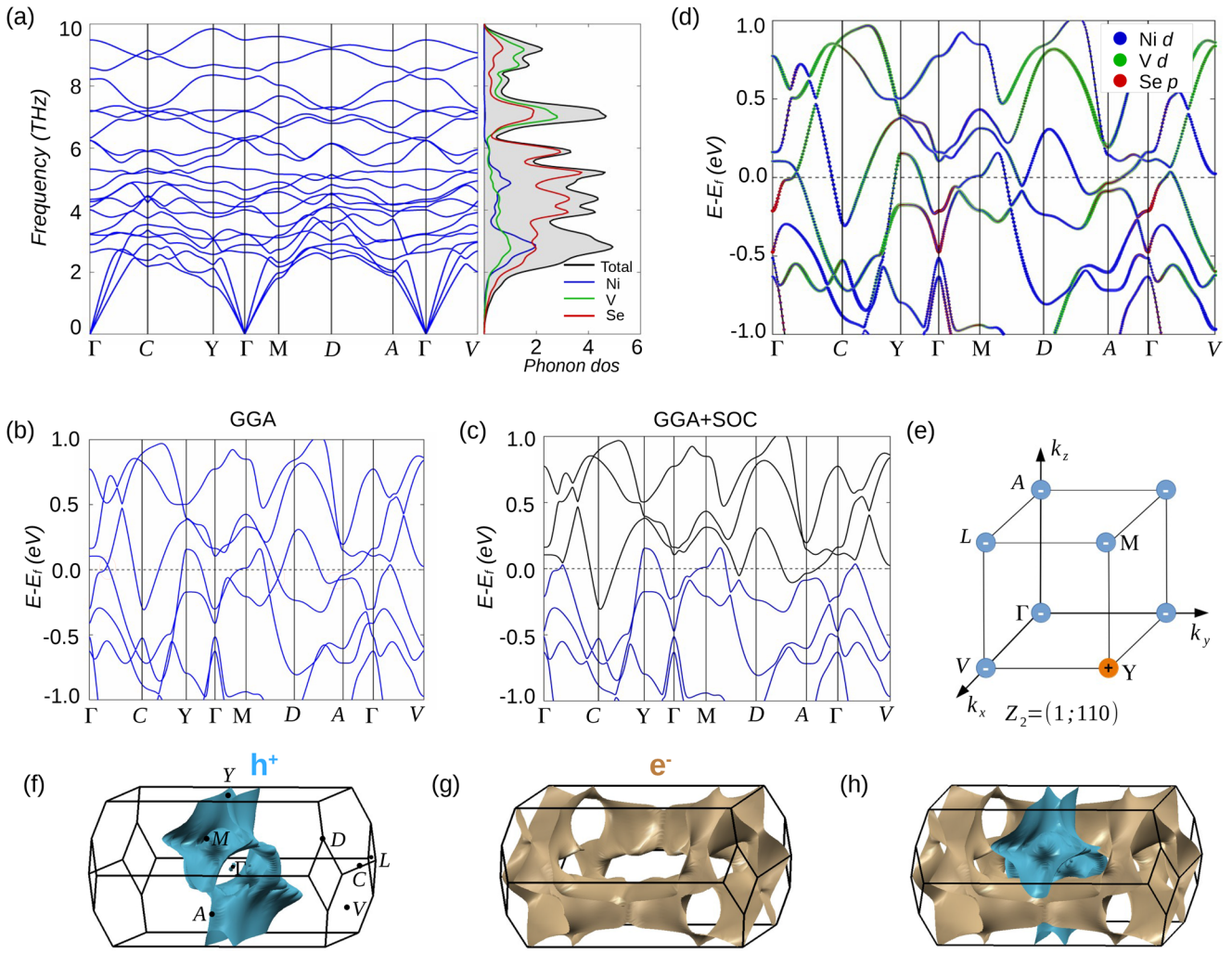

Figure 2. a) Calculated phonon dispersion and total and partial phonon density of states of bulk NiV_2Se_4. The low-frequency phonons mainly arise from Ni and Se atoms whereas high-frequency phonons arise from V and Se atoms. Bulk band structure b) without and c) with spin-orbit coupling (SOC). The nodal band crossings along high-symmetry directions are highlighted with red circles in (b). These crossing points are gapped in (c), leading to a local band gap between valence (blue lines) and conduction (black lines) bands. d) Orbital resolved band structure with SOC. Blue, green, and red markers identify Ni *d*, V *d*, and Se *p* states, respectively. e) Parity eigenvalues of the occupied bands at eight time-reversal invariant momentum points. f,g) Calculated individual Fermi pockets and h) the Fermi surface of NiV_2Se_4.

also agrees with Bouchard et al. (1966),[21] who first reported an anomaly at about 160 K in $\rho(T)$ of a polycrystalline sample of NiV_2Se_4. They suggested that the observed anomaly may be due to either a crystallographic or a magnetic transition. However, we find that the broad anomaly between 150 and 200 K cannot be ascribed to a structural transition, since our diffraction studies did not find any evidence for it (Section 2.1). Explanations for these features could be the development of spin fluctuations or CDW fluctuations as opposed to long-range magnetic order or CDW ordering. The latter involve structural distortions, like in CuV_2S_4,[9] $BaFe_2Al_9$,[29] and $R_2Ir_3Si_5$ (R = Lu, Er).[30,31]

The metallic behavior of $Ni_{0.85}V_2Se_4$ is consistent with the properties of polycrystalline materials of the defect-NiAs structure.[11–20] Below the broad hump, $\rho(T)$ exhibits an unusual $T^{3/2}$ dependence for 15–150 K. Such a behavior is generally observed in spin glasses and amorphous ferromagnets, where a $T^{3/2}$ dependence in $\rho(T)$ is the result of a diffusive motion of the charge carriers.[32,33] Most theories suggest an explanation of the anomalous resistivity by an inhomogeneous magnetic state, through comparison with the resistivity of spin glasses.[34] Since $Ni_{0.85}V_2Se_4$ is a single crystal, the diffusive carrier motion has to be intrinsic somewhat similar to the behavior observed in MnSi under pressure.[35]

It is well-established that the electronic properties of metals on the border of magnetic phase transitions at low temperatures are often found to exhibit temperature dependencies that differ from the predictions of Fermi liquid theory. Early attempts to explore such non-Fermi-liquid behavior have been based on mean-field treatments of the effects of enhanced magnetic fluctuations, as in the self-consistent renormalization (SCR) model.[36] The SCR model seems to explain the temperature dependence of the resistivity of Ni_3Al at high pressures, where its ferromagnetism is suppressed, leading to a negligible magnetic correlation vector $\kappa(T)$. In the idealized limit $\kappa \to 0$ and $T \to 0$, the SCR model predicts

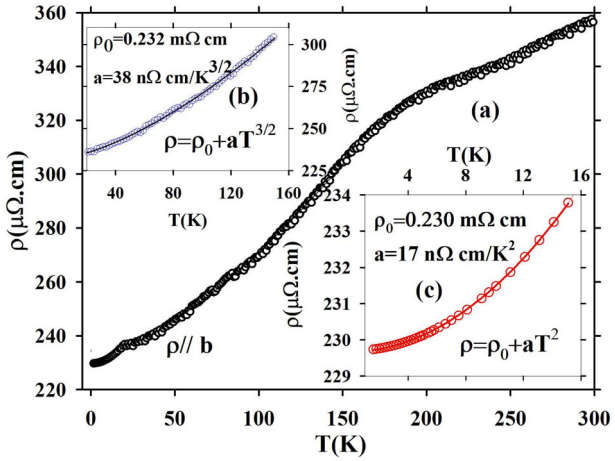

Figure 3. Electrical resistivity of $Ni_{0.85}V_2Se_4$. Curve (a) $\rho(T)$ for the whole measured range of temperatures 1.5–300 K. Curve (b), upper inset, provides an expanded view of 15–150 K; the solid line is a fit to a $T^{3/2}$ dependence (Equation (1)), with $\rho_{0,1}$ = 231.600 (1) μΩ,cm and a_1 = 0.038 (1) μΩ,cm $K^{-3/2}$. Curve (c), lower inset, gives an expanded view of 1.5–15 K; the solid line is a fit to a T^2 dependence (Equation (2)), with $\rho_{0,2}$ = 229.982 (1) μΩ,cm and a_2 = 0.017 (1) μΩ,cm K^{-2}.

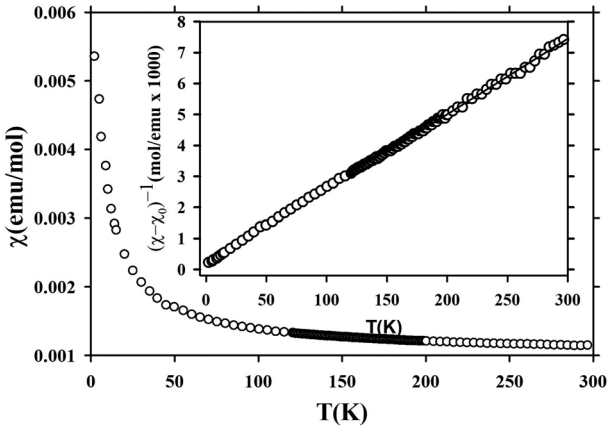

Figure 4. Temperature dependence of the magnetic susceptibility of $Ni_{0.85}V_2Se_4$. Data measured in a field of 5 T under zero-field cooled (ZFC) conditions. A measurement under field cooled (FC) conditions produced data coinciding with those shown for ZFC conditions. The inset provides the inverse susceptibility; the solid line is a fit to the modified Curie–Weiss law (Equation (3)), with χ_0 = 1.01 (1) × 10^{-3},emu mol^{-1}, C = 0.040 (1),emu mol^{-1} K^{-1}, μ_{eff} = 0.57 (1) μ_B and θ = 4.8 (1) K.

that in 3D, the quasiparticle scattering rate $(\tau_{qp})^{-1}$ varies linearly with the quasiparticle excitation energy, rather than quadratically as in the standard Fermi-liquid picture. This form of $(\tau_{qp})^{-1}$ is similar to that of the marginal Fermi-liquid model,[37] which is normally associated with a linear temperature dependence of the resistivity. However, at the border of ferromagnetism, the relevant fluctuations responsible for quasiparticle scattering are of long wavelength and, thus, are ineffective in reducing the current. This leads to a transport relaxation rate $(\tau_{tr})^{-1}$ that differs from $(\tau_{qp})^{-1}$ and is not linear in T. Instead, it varies as $T^{5/3}$, which was observed in high pressure studies on Ni_3Al.

For a metal on the border of metallic antiferromagnetism in 3D, the SCR model predicts $\rho(T)$ to vary as $T^{3/2}$ in the idealized limit $\kappa \to 0$, $T \to 0$, where $\kappa(T)$ now stands for the correlation wave vector for the staggered magnetization. This simple model for the scattering from antiferromagnetic fluctuations assumes that the scattering rate can be averaged over the Fermi surface. Within the SCR model, this procedure would seem to require the presence of a sufficient level of defects, the latter which might be provided by the chemical disorder due to vacancies at the A-site in $Ni_{0.85}V_2Se_4$. This site vacancy is supposed to inhibit the short circuiting caused by the carriers on the cold spots of the Fermi surface, that is, regions far from the hot spots connected by the antiferromagnetic ordering wave vector and, thus, strongly affected by spin-fluctuation scattering. Such a behavior has been observed in NiSSe.[38]

In the case of single crystalline $Ni_{0.85}V_2Se_4$, the temperature dependence of the electrical resistivity between 15 and 150 K could be fitted by (upper inset (b) of Figure 3)

$$\rho(T) = \rho_{0,1} + a_1 T^{3/2} \quad (1)$$

where $\rho_{0,1}$ is the residual resistivity and the second term is the contribution from scattering proposed by the SCR model. It is of interest to see that below 15 K, $\rho(T)$ can be described by (lower inset (c) of Figure 3)

$$\rho(T) = \rho_{0,2} + a_2 T^2 \quad (2)$$

which suggests that the anomalous temperature dependence ceases to exist below 15 K. The second term in Equation (2) arises from the scattering of electrons due to localized spin fluctuations.[39]

2.4. Magnetic Susceptibility

The temperature dependence of the magnetic susceptibility clearly shows paramagnetic behavior (**Figure 4**). However, it does deviate from a simple Curie–Weiss behavior, as discussed below. Magnetization measurements performed under field cooled (FC; not shown) and zero-field cooled (ZFC; Figure 4) conditions produced identical results, implying that spin glass phenomena can be ruled out in the case of $Ni_{0.85}V_2Se_4$. The high temperature (150–300 K) data can be described by a modified Curie–Weiss law,

$$\chi = \chi_0 + C/(T + \theta) \quad (3)$$

where χ_0 includes the diamagnetic and temperature-independent paramagnetic contributions. From the value of the Curie constant C, the effective magnetic moment is estimated as μ_{eff} = 0.57 (1) μ_B per formula unit. Usually, the Ni ion does not have a magnetic moment in metallic compounds of the type AT_2X_4, since all valence electrons of Ni are completely delocalized in fully ordered crystal structures. Apparently, this scenario breaks down in $Ni_{0.85}V_2Se_4$, which again might be related to the vacancies on the Ni site. The Weiss temperature is found to be θ = 4.8 (1) K, indicative of weak antiferromagnetic exchange interactions. The inverse susceptibility (Figure 4) shows small deviations from linear behavior below 150 K.

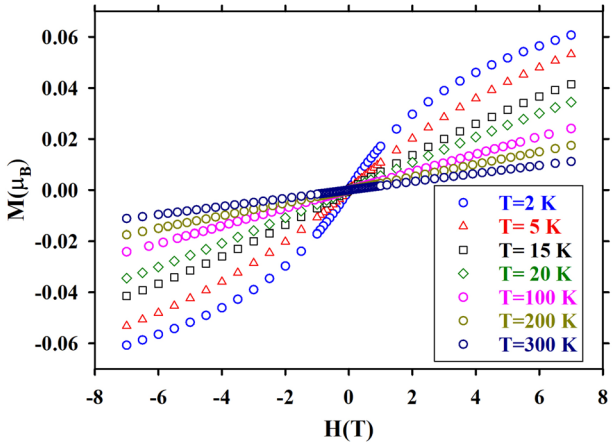

Figure 5. Magnetization (M) in dependence on the applied magnetic field (H) at selected temperatures.

Isothermal magnetization (M–H) curves have been measured at selected temperatures within the range 2–300 K up to magnetic fields of ±7 T (**Figure 5**). Hysteresis is absent at all temperatures, demonstrating that $Ni_{0.85}V_2Se_4$ does not undergo a magnetic phase transition, but remains in the paramagnetic state down to 2 K. At the lowest measured temperatures, the M–H dependence is S-shaped instead of linear at higher temperatures. This might be related to the fact that lower temperatures allow to reach higher values of H/T, thus bringing the M–H relation outside the linear regime. However, attempts failed to bring all data onto a universal H/T dependence. This seems to imply that the crystal does not behave like an usual paramagnet below 15 K.

2.5. Specific Heat

The specific heat, $C_p(T)$, decreases on cooling (**Figure 6**).

The absence of sharp features and the presence of a broad, weak anomaly at T = 150–170 K rule out a possible structural phase transition, which is in agreement with our single-crystal X-ray diffraction data. However, the presence of this anomaly in the specific heat data is in agreement with the anomalies observed in resistivity data. The origin of this anomaly could be attributed to spin or CDW fluctuations. It is important to specify here, that the anomalous temperature dependence of the resistivity ($T^{3/2}$) starts below this transition. The low temperature data can be fitted with the model,[40]

$$C_p/T = \gamma + \beta T^2 + a \ln(T^*/T) \quad (4)$$

The first term is the contribution due to conduction electrons, the second term is the contribution from the lattice, and the third term is the contribution from spin fluctuations due to disorder. This model was successfully employed to explain a similar anomaly in the specific heat of $Fe_{1-x}V_{2+x}Al$ in another context.[40] The fit yields γ = 104.0 (1) mJ mol^{-1} K^{-2} and the Debye temperature θ_D = 252.9 (1) K. The existence of magnetic fluctuations below 15 K has been corroborated by the isothermal magnetization data, as explained earlier. The presence of such magnetic fluctuations seems to change the anomalous temperature dependence of resistivity behavior below 15 K.

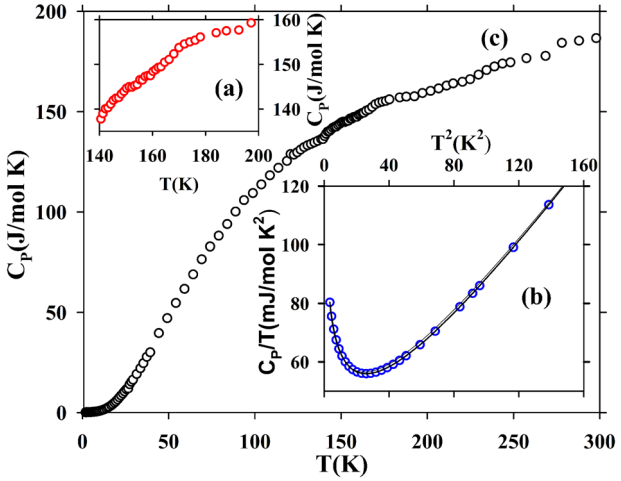

Figure 6. Temperature dependence of the specific heat C_p. Curve (c) displays $C_p(T)$ for temperatures 2–300 K. The upper inset (a) provides an expanded view of the region of the anomaly around 160 K. The lower inset (b) displays C_p/T versus T^2 at low temperatures 2–12 K. Contributions from strong spin fluctuations are demonstrated by a fit (solid line) of Equation (4) to the data, resulting in γ = 104.0 (1) mJ mol^{-1} K^{-2}, β = 0.83 (1) mJ mol^{-1} K^{-4}, θ_D = 252.9 (1) K, a = 20.1 (1) mJ mol^{-1} K^{-2}, and T^* = 0.86 (1) K.

3. Conclusions

The perfectly ordered crystal structure of NiV_2Se_4 does not have a magnetic moment on Ni. However, our attempted growth of single crystals of NiV_2Se_4 has resulted in Ni-deficient crystals, where the crystallographic Ni site has 15% vacancies, but full chemical order is preserved at the V and the two Se sites of the AT_2Se_4 monoclinic structure type. This observation is in agreement with reports in the literature of crystallization attempts, where part or all of the transition metal A can be occupied by defects or V atoms.[21,41]

Single crystalline $Ni_{0.85}V_2Se_4$ is found to be a Z_2 topological metal, that exhibits a cross-over in its physical properties at temperatures around 150 K. All properties, including low-temperature X-ray diffraction data, are in agreement with the absence of phase transitions down to T = 1.5 K in the absence of a magnetic field. The temperature dependence of the electrical resistivity of $Ni_{0.85}V_2Se_4$ is anomalous in the temperature range from 15–150 K, while the presence of magnetic correlations below 15 K probably leads to T^2 dependence of resistivity. It is interesting to compare the present results to the well established Z_2 topological metal RV_6Sn_6 (R = Gd and Y),[42] containing a kagome network of V ions coordinated by Sn and separated by triangular lattice planes of rare-earth ions. The Gd spins contribute to the observed magnetism of GdV_6Sn_6 while YV_6Sn_6 is in a paramagnetic state. Unlike the case of YV_6Sn_6, minor site disorder of Ni in $Ni_{0.85}V_2Se_4$ is responsible for its anomalous low-temperature properties. The broad hump in the resistivity may be related to the anomaly in the specific heat in the temperature range 150–160 K. However, the exact nature of the crossover is not understood at present. These features combine with the gradual build-up of antiferromagnetic fluctuations upon cooling. Isothermal magnetization curves confirm the absence of bulk

magnetic order down to 2 K, but attempts have failed to bring all data onto a universal H/T dependence. This seems to imply that the crystal does not behave like a usual paramagnet below 15 K, and it suggests a build-up of antiferromagnetic correlations. We believe that $Ni_{0.85}V_2Se_4$ is a Z_2 is a topological metal that displays unusual electronic properties due to significant electron correlations. However, to understand this system, one needs more investigations, notably on the nature of the anomalous behavior around 160 K and Fermi surface studies using angle-resolved photoemission spectroscopy.

4. Experimental Section

Crystal Growth and Characterization by EPMA: Attempts to synthesize single-crystalline NiV_2Se_4 resulted in the formation of $Ni_{0.85}V_2Se_4$ prepared by solid-state reaction of the elements in evacuated quartz-glass tubes at a temperature of $T = 1153$ K, employing stoichiometric amounts of the elements obtained from Alfa Aesar: nickel (99.996% purity), vanadium (99.5%), and selenium (99.999%). Single crystals had been grown by vapor transport in evacuated quartz-glass tubes, employing iodine as transport agent and a temperature gradient of $T = 1033 / 973$ K over 200 mm. The chemical composition had been determined as $Ni_{0.925(9)}V_{2.054(7)}Se_4$ by an electron probe micro-analyzer (EPMA). These values were the average over 57 points measured on a flat, as-grown surface sliced off from the large single crystal used for the physical-properties measurements. The finding agreed with the results of X-ray diffraction (see Section 2.1).

Temperature Dependent Single-Crystal X-Ray Diffraction (SXRD): SXRD had been measured on a mar345dtb image plate diffractometer (marXperts, Germany) with Ag-Kα radiation from a rotating anode generator. Initially, several crystals from the batch were tested, all showing that they were Ni deficient similar to what had been found with EPMA. For the final reported measurement a crystal of dimensions $0.1 \times 0.1 \times 0.1$ mm^3 was crushed from the large crystal which was used for physical properties measurements.

A complete set of diffraction images had been measured at temperatures 298 and 100 K, employing an exposure time such that the strongest Bragg's reflection was close to the saturation of the detector. A second run was measured with an offset of 30° in 2θ for obtaining data at high resolution, and employing an eight times longer exposure time, resulting in overexposed strong reflections but allowing for detection of weak scattering effects. Superlattice reflections could not be detected, in agreement with the absence of a CDW at 100 K. Details are given in Section S1 and S2, Supporting Information.[26]

Physical Property Measurements: The electrical resistivity $\rho(T)$ had been measured on cooling from 300 down to 1.5 K in a standard four-probe configuration, employing a cryostat and a LR-700 (Linear Research, USA) bridge with 5 mA current of small AC frequency of 16 Hz. Electrical contacts had been made using silver paste and gold wires (40 µm diameter). The magnetic susceptibility $\chi(T)$ had been measured for temperatures 2–300 K, using a commercial SQUID magnetometer (MPMS5 by Quantum Design, USA). Measurements had been repeated in both zero-field-cooled (ZFC) and field-cooled (FC) conditions for magnetic fields of different strength. The isothermal magnetization had been measured for magnetic fields from −7 to +7 Tesla at a few selected temperatures. The heat capacity $C_p(T)$ had been measured from 2 to 300 K by the thermal relaxation method using a physical property measuring system (PPMS, Quantum Design, USA).

Density Functional Theory Calculations: Electronic structure calculations were performed using the Vienna ab initio simulation package (VASP)[43] with the projector augmented (PAW)[44] wave method. Generalized gradient approximation of Perdew, Burke, and Ernzerhof (PBE)[45] was used to include the exchange-correlation effects. An energy cutoff of 380 eV was used for the plane wave basis and a $10 \times 10 \times 10$ Γ centered k-mesh was employed for the Brillouin zone (BZ) sampling. Experimental lattice parameters with fully optimized ionic positions were considered in the computations. Atomic positions were optimized until the residual forces on each atom were less than 0.0001 eV Å^{-1}. The material-specific tight-binding Hamiltonian[46,47] was generated to compute the topological properties using the WannierTools[48] package. The Xcrysden program was used to visualize the Fermi surface.[49] The phonon spectrum was obtained using the frozen phonon method as implemented in the Phonopy[50] code with a $2 \times 2 \times 2$ supercell.

Supporting Information

Supporting Information is available from the Wiley Online Library or from the author.

Acknowledgements

Single crystals had been grown by Kerstin Küspert at the Laboratory of Crystallography in Bayreuth. The authors thank Detlef Krauße of the Bavarian Geoinstitute (BGI) in Bayreuth for performing the electron microprobe experiments. This research had been funded by the Deutsche Forschungsgemeinschaft (DFG, German Research Foundation)–265092781. S.M. thanks the Tata Institute of Fundamental Research Mumbai for providing a postdoctoral fellowship and VGST CESEM GRD-852. The work at TIFR was supported by the Department of Atomic Energy of the Government of India under Project No. 12-R&D-TFR-5.10-0100.

Open access funding enabled and organized by Projekt DEAL.

Conflict of Interest

The authors declare no conflict of interest.

Data Availability Statement

The data that support the findings of this study are available from the corresponding author upon reasonable request.

Keywords

charge-density-waves, non Fermi liquids, topological metals, vacancies

Received: November 25, 2022
Revised: April 18, 2023
Published online: May 9, 2023

[1] S. Li, Z.-M. Yu, Y. Yao, S. A. Yang, *Front. Phys.* **2020**, *15*, 43201.
[2] B. Singh, H. Lin, A. Bansil, *Adv. Mater.* **2022**, *2022*, 2201058.
[3] T. Hagino, Y. Seki, N. Wada, S. Tsuji, T. Shirane, K. I. Kumagai, S. Nagata, *Phys. Rev. B* **1995**, *51*, 12673.
[4] S. Nagata, T. Hagino, Y. Seki, T. Bioth, *Phys. B* **1994**, *194–196*, 1077.
[5] T. Furubayashi, T. Matsumoto, T. Hagino, S. Nagata, *J. Phys. Soc. Jpn* **1994**, *63*, 3333.
[6] T. Sekine, K. Uchinokura, H. Iimura, R. Yoshizaki, E. Matsuura, *Solid State Commun.* **1984**, *51*, 187.
[7] J. Mahy, D. Colaitis, D. van Dyck, S. Amelinckx, *J. Solid State Chem.* **1987**, *68*, 320.
[8] P. G. Radaelli, Y. Horibe, M. J. Gutmann, M. Ishibashi, C. H. Chen, R. M. Ibberson, M. Koyama, Y. S. Hor, V. Kiryukhin, S. W. Cheong, *Nature* **2002**, *416*, 155.
[9] S. Ramakrishnan, A. Schönleber, C. B. Hübschle, C. Eisele, A. M. Schaller, T. Rekis, N. H. A. Bui, F. Feulner, S. van Smaalen, B. Bag, S. Ramakrishnan, M. Tolkiehn, C. Paulmann, *Phys. Rev. B* **2019**, *99*, 195140.

[10] A. Wold, K. Dwight, *Solid State Chemistry: Synthesis, Structure, and Properties of Selected Oxides and Sulfides*, Chapman & Hall, New York **1993**, pp. 227–234.
[11] R. J. Bouchard, *Inorg. Chem.* **1969**, *8*, 850.
[12] F. Jellinek, *Acta Crystallogr.* **1957**, *10*, 620.
[13] A. V. Powell, D. C. Colgan, C. Ritter, *J. Solid State Chem.* **1997**, *134*, 110.
[14] A. V. Powell, C. Ritter, P. Vaqueiro, *J. Solid State Chem.* **1999**, *144*, 372.
[15] P. Vaqueiro, A. V. Powell, A. I. Coldea, C. A. Steer, I. M. Marshall, S. J. Blundell, J. Singleton, T. Ohtani, *Phys. Rev. B* **2001**, *64*, 132402.
[16] R. H. Plovnick, D. S. Perloff, M. Vlasse, A. Wold, *J. Phys. Chem. Solids* **1968**, *29*, 1935.
[17] B. L. Morris, P. Russo, A. Wold, *J. Phys. Chem. Solids* **1970**, *31*, 635.
[18] B. L. Morris, R. H. Plovnick, A. Wold, *Solid State Commun.* **1969**, *7*, 291.
[19] P. Vaqueiro, M. Bold, A. V. Powell, C. Ritter, *Chem. Mater.* **2000**, *12*, 1034.
[20] Y. K. Kuo, K. M. Sivakumar, J. Y. Lin, C. N. Kuo, C. S. Lue, *J. Phys.: Condens. Matter* **2007**, *19*, 216210.
[21] R. J. Bouchard, A. Wold, *J. Phys. Chem. Solids* **1966**, *27*, 591.
[22] A. M. M. Schreurs, X. Xian, L. M. J. Kroon-Batenburg, *J. Appl. Crystallogr.* **2010**, *43*, 70.
[23] G. M. Sheldrick, *SADABS, Version 2008/1*, University of Göttingen, Göttingen **2008**.
[24] R. J. Bouchard, W. T. Robinson, A. Wold, *Inorg. Chem.* **1966**, *5*, 977.
[25] V. Petricek, M. Dusek, L. Palatinus, *Z. Kristallogr.* **2014**, *229*, 345.
[26] See Supporting Information at [URL will be inserted by publisher] for details on the diffraction experiments at 100 K, reconstructed reciprocal images, and additional information on band-structure calculations.
[27] *International Tables for Crystallography* (Ed.: T. Hahn), Vol. *A*, 5th ed., Kluwer Academic Publishers, Dordrecht **2006**.
[28] L. Fu, C. L. Kane, *Phys. Rev. B* **2007**, *76*, 045302.
[29] W. R. Meier, B. C. Chakoumakos, S. Okamoto, M. A. McGuire, R. P. Hermann, G. D. Samolyuk, S. Gao, Q. Zhang, M. B. Stone, A. D. Christianson, B. C. Sales, *Chem. Mater.* **2021**, *33*, 2855.
[30] S. Ramakrishnan, A. Schönleber, J.-K. Bao, T. Rekis, S. R. Kotla, A. M. Schaller, S. van Smaalen, L. Noohinejad, M. Tolkiehn, C. Paulmann, N. S. Sangeetha, D. Pal, A. Thamizhavel, S. Ramakrishnan, *Phys. Rev. B* **2021**, *104*, 054116.
[31] S. Ramakrishnan, A. Schönleber, T. Rekis, N. van Well, L. Noohinejad, S. van Smaalen, M. Tolkiehn, C. Paulmann, B. Bag, A. Thamizhavel, D. Pal, S. Ramakrishnan, *Phys. Rev. B* **2020**, *101*, 060101(R).
[32] J. A. Hertz, *Phys. Rev. B* **1976**, *14*, 1165.
[33] A. J. Millis, *Phys. Rev. B* **1993**, *48*, 7183.
[34] J. A. Mydosh, *Spin Glasses: An Experimental Introduction*, Taylor and Francis, London**1993**.
[35] C. Pfleiderer, G. J. McMullan, S. R. Julian, G. G. Lonzarich, *Phys. Rev. B* **1997**, *55*, 8330.
[36] P. G. Niklowitz, F. Beckers, G. G. Lonzarich, G. Knebel, B. Salce, J. Thomasson, N. Bernhoeft, D. Braithwaite, J. Flouquet, *Phys. Rev. B* **2005**, *72*, 024424.
[37] C. M. Varma, P. B. Littlewood, S. Schmitt-Rink, E. Abrahams, A. E. Ruckenstein, *Phys. Rev. Lett.* **1989**, *63*, 1996.
[38] S. Miyasaka, H. Takagi, Y. Sekine, H. Takahashi, N. Mori, R. J. Cava, *J. Phys. Soc. Jpn.* **2000**, *69*, 3166.
[39] A. Kaiser, *Phil. Mag. B* **1992**, *65*, 1197.
[40] A. T. Lonchakov, V. V. Marchenkov, V. I. Okulov, K. A. Okulova, T. E. Govorkova, S. M. Podgornykh, H. W. Weber, *J. Phys.: Conf. Ser.* **2014**, *568*, 052018.
[41] K. Kallel, H. Boller, *J. Less-Common Met.* **1984**, *102*, 213.
[42] G. Pokharel, S. M. L. Teicher, B. R. Ortiz, P. M. Sarte, G. Wu, S. Peng, J. He, R. Seshadri, S. D. Wilson, *Phys. Rev. B* **2021**, *104*, 235139.
[43] G. Kresse, J. Furthmüller, *Phys. Rev. B* **1996**, *54*, 11169.
[44] P. E. Blöchl, *Phys. Rev. B* **1994**, *50*, 17953.
[45] J. P. Perdew, K. Burke, M. Ernzerhof, *Phys. Rev. Lett.* **1996**, *77*, 3865.
[46] N. Marzari, D. Vanderbilt, *Phys. Rev. B* **1997**, *56*, 12847.
[47] A. A. Mostofi, J. R. Yates, Y.-S. Lee, I. Souza, D. Vanderbilt, N. Marzari, *Comput. Phys. Commun.* **2008**, *178*, 685.
[48] Q. Wu, S. Zhang, H.-F. Song, M. Troyer, A. A. Soluyanov, *Comput. Phys. Commun.* **2018**, *224*, 405.
[49] A. Kokalj, *J. Mol. Graphics Modell.* **1999**, *17*, 176.
[50] A. Togo, I. Tanaka, *Scr. Mater.* **2015**, *108*, 1.